FEBS Letters

FEBS PRESS science publishing by scientists

Oct motif variants in Beckwith–Wiedemann syndrome patients disrupt maintenance of the hypomethylated state of the *H19/IGF2* imprinting control region

Shuichi Kubo, Chihiro Murata, Hanayo Okamura, Taku Sakasegawa, Chiye Sakurai, Kiyotaka Hatsuzawa and Naohiro Hori

Division of Molecular Biology, Faculty of Medicine, School of Life Sciences, Tottori University, Yonago, Japan

Correspondence
H. Naohiro, Division of Molecular Biology, School of Life Sciences, Faculty of Medicine, Tottori University, Yonago, Tottori 683-8503 Japan
Tel: +81 859 38 6203
E-mail: horinao@tottori-u.ac.jp

(Received 26 September 2019, revised 27 December 2019, accepted 20 January 2020, available online 17 February 2020)

doi:10.1002/1873-3468.13750

Edited by Judith Zaugg

The methylation status of imprinting control center 1 (IC1) regulates the monoallelic transcription of *H19* and *Igf2* in mammalian cells. Several single nucleotide variants in Oct motifs within IC1 occur in patients with Beckwith–Wiedemann syndrome (BWS) who have hypermethylated maternal IC1. However, the importance of Oct motifs in the regulation of IC1 methylation status remains unclear. Here, we demonstrate that three variants found in BWS (BWS variants) suppress intensive induction of DNA demethylation, whereas consensus disruption of motifs unrelated to BWS only slightly affects the induction of demethylation. BWS variants reduce DNA demethylation levels and trigger the accumulation of DNA methylation downstream of the IC1 transgenes. Thus, the risk of IC1 hypermethylation is associated with inhibitory levels of Oct motif-dependent hypomethylation maintenance activities.

Keywords: Beckwith–Wiedemann syndrome; CTCF-binding site; DNA demethylation; imprinting control center 1; Oct motif-dependent regulation; P19 cell

Genomic imprinting is a transcriptional control mechanism based on the epigenetic modification of differentially methylated regions (DMR) found in organized gene clusters [1–3]. In humans, ~ 100 genes (http://www.geneimprint.com) are controlled by genomic imprinting. The loss of imprinting is associated with the onset of various genetic diseases. The imprinted gene domain *H19*/*insulin-like growth factor 2* (*IGF2*) is located on the human chromosome 11p15.5 locus. It encompasses ~ 5 kb DMR (imprinting centers 1 or IC1) at 2 kb upstream of *H19*. Human IC1 (hIC1) includes seven CCCTC-binding factor (CTCF) binding sites (CBSs). It uses CTCF protein binding to control monoallelic *H19* and *IGF2* transcription depending on changes in enhancer accessibility [4–6]. CTCF binds to maternally derived hypomethylated IC1 but not to paternally derived hypermethylated IC1. DNA methylation on the core motif of CBS prevents the binding of CTCF proteins [7,8]. Hypermethylation of paternal IC1 directs the enhancer toward *IGF2*. In contrast, hypomethylation of maternal IC1 enhances *H19* transcription *via* CTCF-dependent alterations in chromosome structure [6]. Parent-of-origin-dependent IC1 methylation is established during gametogenesis and is maintained after fertilization [9].

Spatial organization of the *H19*/*Igf2* domain is conserved on mouse distal chromosome 7. The 2-kb mouse IC1 (mIC1) is structurally distinct from hIC1.

Abbreviations
BWS, Beckwith–Wiedemann syndrome; CBS, CTCF-binding site; CTCF, CCCTC-binding factor; dhD1, downstream hD1; dhIC1, downstream region of human IC1; hD1, human dyad octamer motif sequence 1; hIC1, human IC1; IC1, imprinting control center 1; mIC1, mouse IC1; MSRE-PCR, methylation-sensitive restriction enzyme–PCR; OCT3/4, octamer-binding transcription factor 3/4; SD, standard deviation; SO motif, Sox-Oct motif; SOX2, SRY-box containing gene 2; uhD1, upstream hD1.

However, parent-of-origin IC1 methylation (or paternal hypermethylation and maternal hypomethylation) is conserved in humans and mice. The pluripotency-related transcription factor SRY-box containing gene 2 (SOX2) and the octamer-binding transcription factor 3/4 (OCT3/4) binding sites (7-bp Sox motif and 8-bp Oct motif) are well conserved between both species [10]. The human *H19*/*IGF2* domain has the 59-bp elements hD1 and hD2 composed mainly of two Sox-Oct motif-like sequences (SO motifs) and a single Oct motif (rO) [10]. The hD1 and hD2 occur in hIC1 and are accompanied by triple-repeat sequences containing CBS1-3 or CBS4-6 (Fig. 1A). In contrast, mIC1 has only one unit composed of two SO motifs at the central portion of the four CBSs. Several studies on mIC1 showed that the four CBSs are required to maintain its hypomethylated status during mouse development [7,8]. After implantation, SO motif mutation or deletion increases DNA methylation in the region surrounding the SO motif containing ≥ 1 CBS in the maternal mIC1 [11,12]. Defects in the CBS or SO motifs do not affect DNA methylation status in paternally derived mIC1 *in vivo*. Collaboration between the CBSs and SO motifs is necessary for the complete maintenance of maternal mIC1 hypomethylation [11,12]. We previously demonstrated that a 160-bp fragment containing SO motifs induces DNA demethylation. Binding defects in the SOX2 and OCT3/4 complexes on the SO motifs suppressed this activity in the mouse embryonic carcinoma cell line P19 [13]. SO motif-dependent demethylation occurs in a wide range of mIC1 and protects them from the accumulation of methylated DNA. Thus, SO motifs defend maternal mIC1 against *de novo* DNA methylation during mouse development. Few studies have focused on the control of hIC1 methylation *via* hD1 or hD2. The latter two may induce DNA demethylation and maintain hIC1 hypomethylation but their modes of action remain to be elucidated.

Beckwith–Wiedemann syndrome (BWS: OMIM 130650) is a congenital overgrowth disorder characterized by macrosomia, macroglossia, and abdominal wall defects [14,15]. Most cases of BWS are accompanied by epigenetic changes in the imprinting control regions *H19*/*IGF2* (IC1) and *KIP2*/*LIT1* (IC2) separately located on human chromosome 11p15.5 [16,17]. Maternal hIC1 hypermethylation and biallelic activation of IGF2 are risk factors for Wilms' tumor and are observed in 5–7% of all BWS patients. However, the hypermethylation mechanisms are unknown [16,17].

Several reports showed that single nucleotide variations in hIC1 are selectively detected in hIC1-hypermethylated BWS patients. On the other hand, the association of these variations with maternal IC1 hypermethylation is obscure as many of them occur as single nucleotide polymorphisms (SNPs) between BWS patients and the healthy population [18]. Several single -nucleotide variants distinct from SNPs are concentrated in hD1, all of which are localized to the rO or Oct motif in one of the two SO motifs (Fig 1A; O1). They contribute to the binding defect in the OCT4/SOX2 complex [19–23]. Patients with BWS who have hIC1 hypermethylation emerge from the maternal inheritance of Oct motif variants. The hD1 element might maintain hypomethylation status by inducing DNA demethylation and/or protecting existing hypomethylation. In BWS patients, aberrant hIC1 methylation may be the result of this activity and it may depend on Oct motif variants. However, the influence of Oct motif variants is unknown as hIC1 hypermethylation is also observed in BWS patients without mutations at or near hIC1 [24].

In the present study, we focused on hD1 variants in BWS patients to elucidate whether the variants directly resulted in the change of DNA methylation status. Toward this goal, we constructed an assay system using P19 cells and estimated the potency of hD1-dependent DNA methylation status regulatory activity. Then, we tested the influence of BWS variants in hD1 on the state of hIC1 methylation of the transgenes integrated into single chromosome locus with MSRE-PCR and bisulfite sequencing method. We propose that hD1 protects hIC1 from the accumulation of

Fig. 1. The 59-bp hD1-containing elements induce Oct motif-dependent DNA demethylation in P19 cells. (A) Structural map of human *H19*-IC1 (IC1). Top: *H19* and *IGF2* loci. Shaded box indicates IC1 (IC1). Middle: expanded map showing *H19* upstream region including hD0, hD1, and hD2 (diamond box) and seven CTCF-binding sites (horizontal lines; CBS1–7). Two different repeat sequences are indicated by gray or white gradation boxes. Bottom: alignment of the hD1 and hD2 sequences encompassing the Sox-Oct motif-like and mouse Sox-Oct motif-containing sequences. Sox motif and Sox motif-like sequence, white box; Oct motif and Oct motif-like sequence, gray box. (B) Restriction map and fragments in the Southern hybridization analysis. Sa, *Sac*I; H, *Hpa*II; fr, fragment. *Hpa*II restriction sites are present in the plasmid vector. (C) Sequences of hD1 and O1O2-mutated hD1. Shaded boxes indicate sequence mutations. (D) Demethylation activity of uhD1 and dhD1. Left: Southern hybridization analysis of hD1 and O1O2m hD1. Results of three biological replicates are shown. Right: plot of DNA demethylation. Demethylation activity was calculated as the ratio of the radioactive count of fr. 3 to total (fr. 1-6) radioactive counts. Data were analyzed using Welch's t-test. ***$P < 0.005$. Error bars represent standard deviation (SD). *P*-values are listed under the plot.

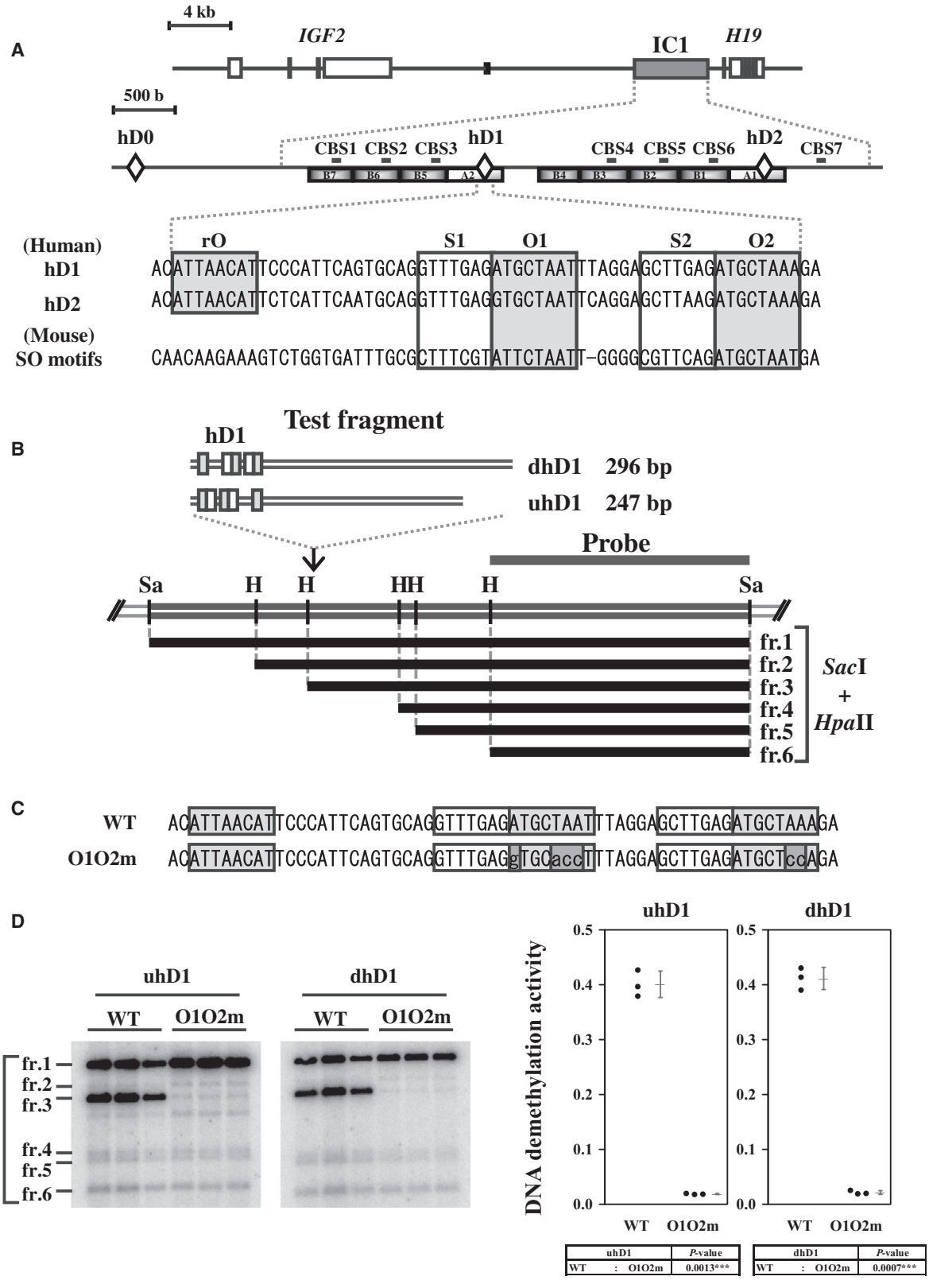
A
4 kb
IGF2
IC1
H19
500 b
hD0
CBS1 CBS2 CBS3
hD1
CBS4 CBS5 CBS6
hD2
CBS7
B7 B6 B5 A2 B4 B3 B2 B1 A1
(Human)
hD1
hD2
(Mouse)
SO motifs
rO
S1
O1
S2
O2
ACATTAACATTCCCATTCAGTGCAGGTTTGAGATGCTAATTTAGGAGCTTGAGATGCTAAAGA
ACATTAACATTCTCATTCAATGCAGGTTTGAGGTGCTAATTCAGGAGCTTAAGATGCTAAAGA
CAACAAGAAAGTCTGGTGATTTGCGCTTTCGTATTCTAATT-GGGGCGTTCAGATGCTAATGA
B
Test fragment
hD1
dhD1 296 bp
uhD1 247 bp
Probe
Sa H H HH H Sa
fr.1
fr.2
fr.3
fr.4
fr.5
fr.6
SacI + HpaII
C
WT ACATTAACATTCCCATTCAGTGCAGGTTTGAGATGCTAATTTAGGAGCTTGAGATGCTAAAGA
O1O2m ACATTAACATTCCCATTCAGTGCAGGTTTGAGgTGCaccTTTAGGAGCTTGAGATGCTccAGA
D
uhD1
dhD1
WT O1O2m WT O1O2m
SacI + HpaII
fr.1
fr.2
fr.3
fr.4
fr.5
fr.6
DNA demethylation activity
0.5
0.4
0.3
0.2
0.1
0.0
WT O1O2m
WT O1O2m
uhD1 P-value
WT : O1O2m 0.0013**
dhD1 P-value
WT : O1O2m 0.0007***

methylation *via* DNA demethylation and that this mechanism is defective in patients with BWS who have Oct motif variants.

Results

hD1 induces demethylation in P19 cells

DNA demethylation mechanisms establish and maintain genomic hypomethylation. We previously showed that a 160-bp element from mIC1 containing SO motifs induces DNA demethylation in P19 cells. Disruption of the Oct3/4 binding consensus sequence (Oct motif) in the SO motifs decreased this activity [13]. The structure of IC1 differs between humans and mice. However, SO motif-like sequences also occur in hIC1 (Fig. 1A). Similarities between these motif-like sequences and the murine consensus SO motif sequence (motif ID: MA0142.1) were scored with JASPR 2018 [25] (Table S1). The scores and relative scores for the two mouse Sox-Oct motifs were 11.471 (0.840) and 12.482 (0.855), respectively. The SO motif-like sequences in hIC1 had relatively high similarity scores. The scores and relative scores for the four human Sox-Oct motif-like motifs were hD1-S1O1, 14.393 (0.882); hD1-S2O2, 8.962 (0.804); hD2-S1O1, 9.167 (0.807); and hD2-S2O2, 6.249 (0.765). The SO motifs in maternal hD1 were either mutated or deleted in BWS patients. These effects were associated with hypermethylation of the maternal hIC1 [19–23]. However, it is unknown whether hD1 has the same demethylation effect in mouse SO motifs (Fig. 1A).

To determine whether hD1 induces DNA demethylation, we cloned hIC1-derived hD1 fragments containing 247-bp upstream or 296-bp downstream sequences (uhD1 and dhD1, respectively; Fig. 1B). We examined demethylation induction by these fragments with or without mutations of the Oct3/4 binding consensus in two Oct motifs of hD1 (WT and O1O2m, respectively; Fig 1C). To explore the induction of DNA demethylation, constructs containing these fragments were methylated *in vitro* with *Hpa*II methyltransferase and transfected into P19 cells. Three days after transfection, Southern blot analysis revealed a decrease in the methylation level at the *Hpa*II. This transient transfection-based assay reveals the degree of DNA demethylation induced by cis-acting sequences in a plasmid that is mainly not integrated into the genomic DNA, although it does not clarify their wide-range regulatory effects because DNA demethylation occurs only at the proximal portion of the cis-acting sequence [13].

WT uhD1 induced demethylation on the proximal *Hpa*II sites in P19 cells, whereas O1O2m uhD1 strongly repressed DNA demethylation ($P = 0.0013$) (Fig. 1D). dhD1 also induced DNA demethylation in a manner dependent on the two Oct motifs ($P = 0.0007$). At least one of the two Oct motifs in hD1 was required for this process.

The Oct motif is crucial for the induction of demethylation in hD1

Sox-Oct motifs are found in conserved in the enhancer of the pluripotency-related gene and regulate gene expression in mouse and human ES cells. Mutation of either the Sox or Oct motif downregulated the luciferase promoter to a similar extent. Thus, both the Sox and Oct motifs are required for transcription in ES cells [26,27]. The Sox- or Oct-family binding consensus elements may be associated with the maintenance of hypomethylation [28]. In the SO motifs of human and mouse IC1, Oct motifs are adjacent to Sox motifs. Several reports in mouse SO motifs showed that the Sox motif was also needed to induce DNA demethylation [10,13].

The SO motif sequences were highly conserved between humans and mice (Fig. 1A). The hD1-dependent DNA demethylation might be controlled by a 15-bp unit. We investigated whether the SO motifs on the hD1 element affect DNA demethylation status. To this end, we used a mutation series manifesting disruption of the consensus-binding sequence (S1m, S2m, O1m, and O2m; Fig. 2A). S1m and O2m slightly reduced the induction of DNA demethylation down to the same level as that of the WT ($P < 0.0001$ and < 0.0001, respectively) (Fig. 2B). Moreover, S2m did not suppress demethylation relative to the WT ($P = 0.1299$). In contrast, only O1m presented with a significant reduction in hD1-dependent DNA demethylation compared with the other motifs ($P < 0.0001$).

BWS variants in Oct motifs disrupt the induction of hD1-dependent DNA demethylation

Patients with BWS who have aberrant maternal hIC1 methylation have various single nucleotide variants or microdeletions in hD1 [19–23]. In hD1, the former is concentrated in the two Oct motifs. To clarify whether the hD1 single nucleotide variants in BWS patients induce DNA demethylation, three variants, AC123789.6: g.80689C>T (C > T), AC123789.6:g.80715T>C (T > C), and AC123789.6: g.80716G>A (G > A), were introduced into hD1 (Fig. 3A). T > C and G > A variants are observed in the O1 motif [19–21]. The C > T variant occurs in the rO motif [22,23]. The BWS variants in both rO and O1 motifs disrupted the induction of

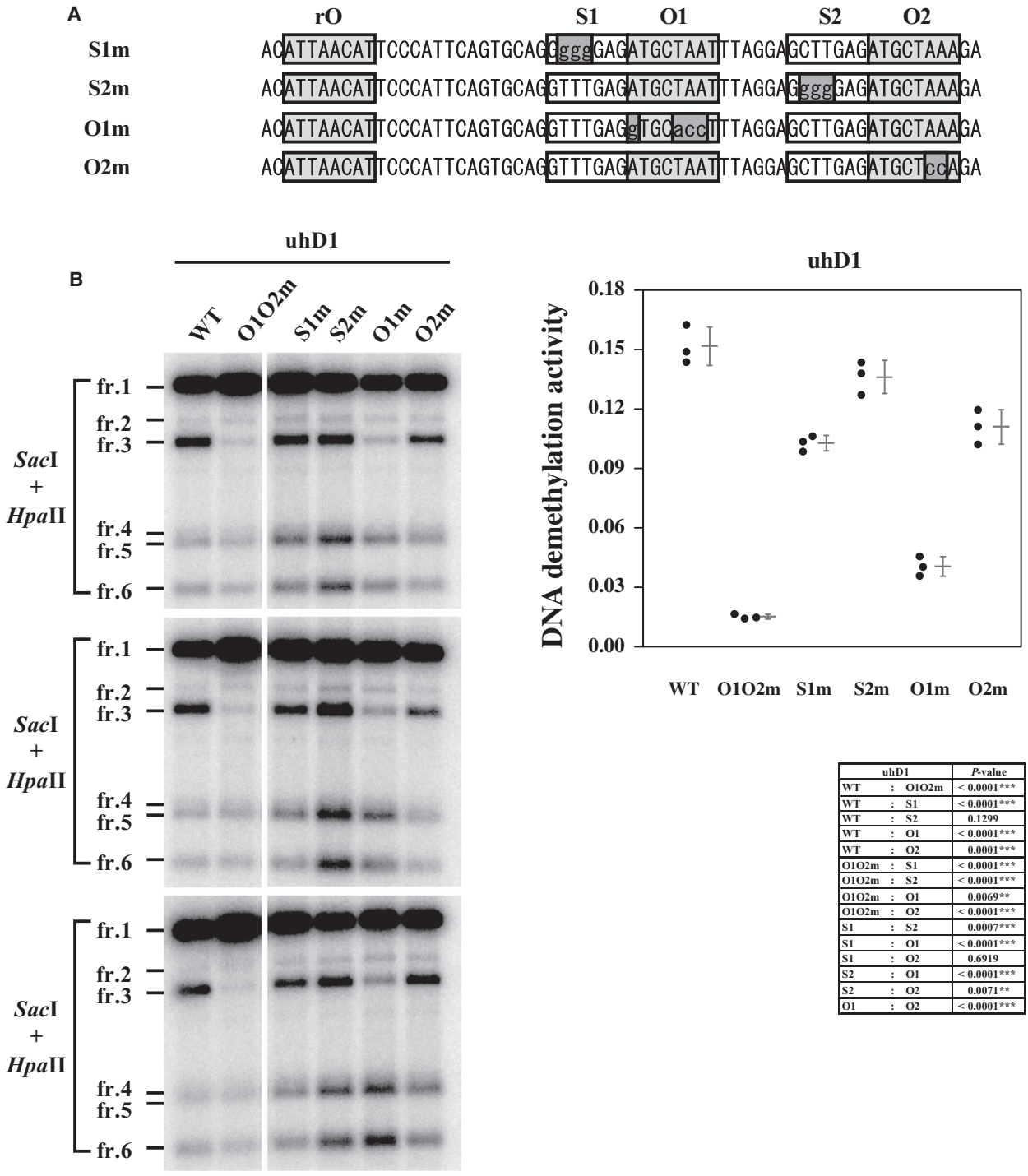

uhD1			*P*-value
WT	:	O1O2m	< 0.0001***
WT	:	S1	< 0.0001***
WT	:	S2	0.1299
WT	:	O1	< 0.0001***
WT	:	O2	0.0001***
O1O2m	:	S1	< 0.0001***
O1O2m	:	S2	< 0.0001***
O1O2m	:	O1	0.0069**
O1O2m	:	O2	< 0.0001***
S1	:	S2	0.0007***
S1	:	O1	< 0.0001***
S1	:	O2	0.6919
S2	:	O1	< 0.0001***
S2	:	O2	0.0071**
O1	:	O2	< 0.0001***

Fig. 2. Mutation of the O1 motif strongly suppresses DNA demethylation relative to other motifs. (A) Consensus mutations of motifs in hD1. Shaded boxes indicate mutations. (B) Effects of consensus mutations on induction of DNA demethylation. Left: Southern hybridization analysis of WT and mutant uhD1. Right: plot of DNA demethylation. Results of three biological replicates are shown. Right: plot of DNA demethylation. Demethylation activity was calculated as the ratio of the radioactive count of fr. 3 to total (fr. 1-6) radioactive counts. Data were analyzed by Tukey's HSD test. ***$P < 0.005$, **$P < 0.01$, *$P < 0.05$. Error bars represent standard deviation (SD). *P*-values are listed under the plot.

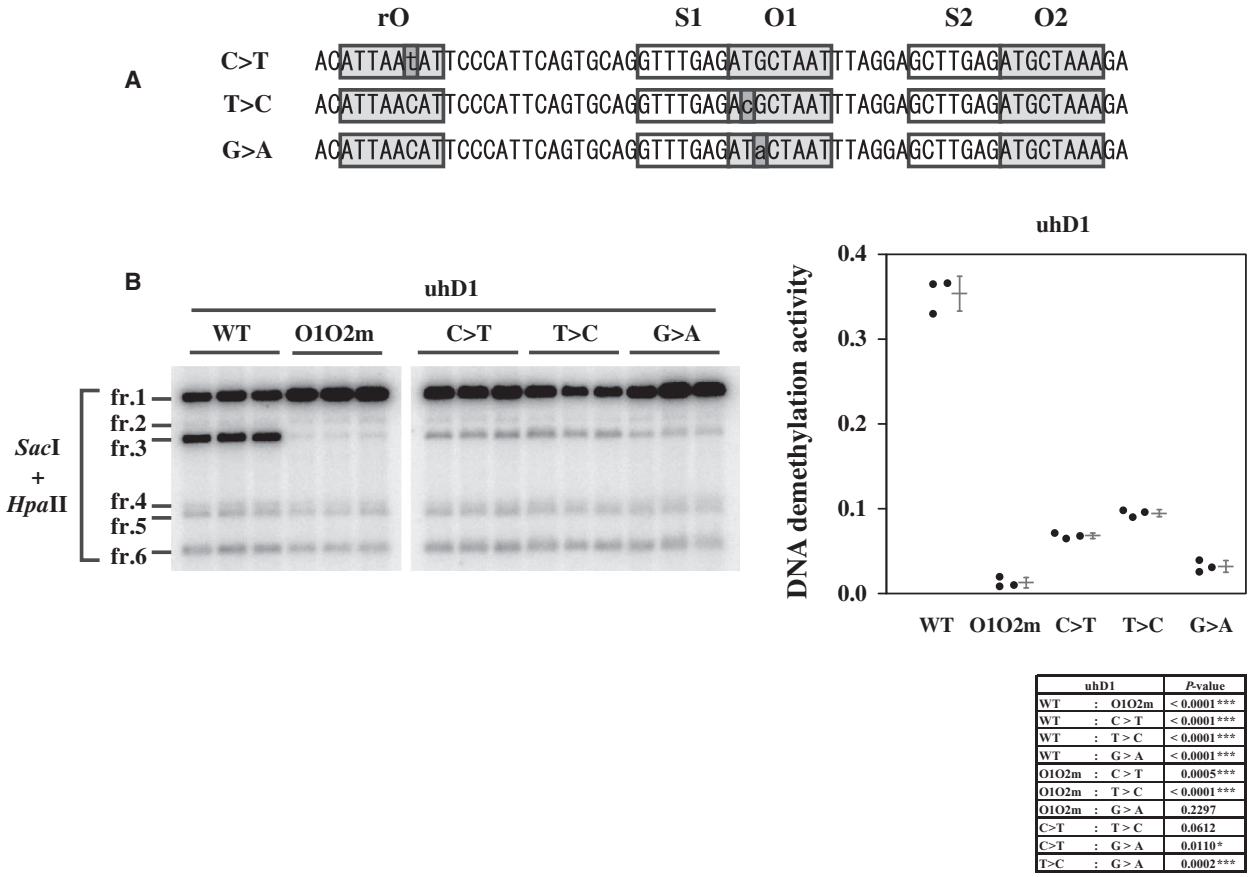

uhD1			*P*-value
WT	:	O1O2m	< 0.0001***
WT	:	C > T	< 0.0001***
WT	:	T > C	< 0.0001***
WT	:	G > A	< 0.0001***
O1O2m	:	C > T	0.0005***
O1O2m	:	T > C	< 0.0001***
O1O2m	:	G > A	0.2297
C>T	:	T > C	0.0612
C>T	:	G > A	0.0110*
T>C	:	G > A	0.0002***

Fig. 3. Oct motif variants in BWS patients strongly inhibit the induction of DNA demethylation. (A) BWS mutations of hD1 used in this assay. Shaded boxes indicate mutations. (B) Effects of BWS mutations on induction of DNA demethylation. Left: Southern hybridization analysis of WT and mutant uhD1. Right: plot of DNA demethylation. Results of three biological replicates are shown. Right: plot of DNA demethylation. Demethylation activity was calculated as the ratio of the radioactive count of fr. 3 to total (fr. 1-6) radioactive counts. Data were analyzed by Tukey's HSD test. ***$P < 0.005$, **$P < 0.01$, *$P < 0.05$. Error bars represent standard deviation (SD). *P*-values are listed under the plot.

hD1-dependent DNA demethylation, although the suppressing effect of variants on DNA demethylation differed (Fig. 3B). The T > C, G > A, and C > T variants significantly downregulated DNA demethylation in P19 cells ($P < 0.0001$, $P < 0.0001$, and $P < 0.0001$, respectively).

Fig. 4. BWS patient variants in Oct motifs inhibit demethylation and promote methylation in dhIC1 in P19 cells. (A) Strategic map estimating alteration of dhIC1 methylation by PCR. Top: Map of Gt(ROSA)26Sor locus in P19-ROSA-L66 cells. e1-e3, exon (shaded boxes). Pur, puromycin gene cassette (white box). Half-solid triangle indicates lox66 site. Striped triangle indicates FAS loxP2 sites. Middle: Expanded map of dhIC1 introduced onto Gt(ROSA)26Sor locus. Human dhIC1 (gray box), neomycin resistance gene (black box), and GFP (solid box) were derived from pL71-dhIC1 introduced by Cre-mediated recombination. Black and white triangles indicate hybrid lox sites formed from recombination between lox66 and lox71. Restriction sites are H (*Hpa*II), Hh (*Hha*I), and MI (*Mlu*I). Open circles and rhombus indicate CTCF-binding sites and Sox-Oct motifs (hD1), respectively. Bottom: Fragments amplified by PCR. Left: amplified fragments and primers. Three fragments (fr. 1–3) were amplified to determine the induction range of hD1-dependent demethylation. Fr. 4 was amplified to correct the quantity of template DNA. Primers are shown by arrows. Right: number of restriction sites in amplified fragments. (B) Estimation of dhIC1 demethylation in BWS mutants. Left: amplified fragments from *Hpa*II-digested WT and mutant dhIC1. Right: methylation status of initially methylated *Hpa*II sites on WT and mutant dhIC1. Results of three biological replicates are shown. Data were analyzed by Tukey's HSD test. ***$P < 0.005$, **$P < 0.01$, *$P < 0.05$. Error bars represent standard deviation (SD). *P*-values are listed right side of the plot. (C) Estimation of dhIC1 *de novo* methylation in BWS mutants. Left: amplified fragments from *Hpa*II, *Hha*I, or *Mlu*I digested WT and mutant dhIC1. Right: methylation level of initially unmethylated restriction sites on the WT and mutant dhIC1. Results of three biological replicates are shown. Data were analyzed by Tukey's HSD test. ***$P < 0.005$, **$P < 0.01$, *$P < 0.05$. Error bars represent standard deviation (SD). *P*-values are listed right side of the plot.

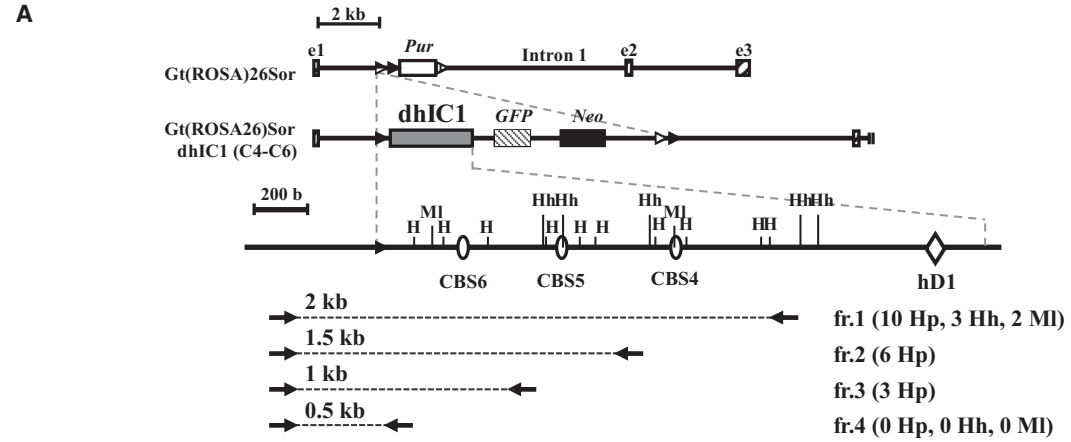

B

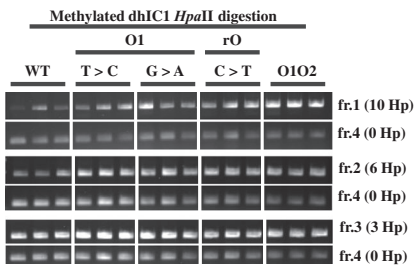

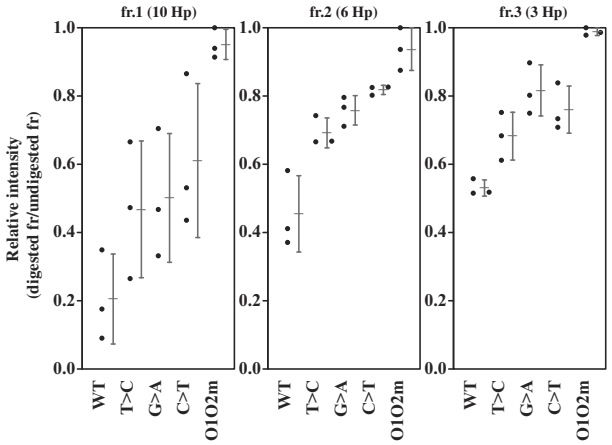

fr.1 (10 Hp)			*P*-value
WT	:	T > C	0.3836
WT	:	G > A	0.2823
WT	:	C > T	0.0903
WT	:	O1O2m	0.0023**
T > C	:	G > A	0.9991
T > C	:	C > T	0.8387
T > C	:	O1O2m	0.0382*
G > A	:	C > T	0.9293
G > A	:	O1O2m	0.0554
C > T	:	O1O2m	0.1816

fr.1 (6 Hp)			*P*-value
WT	:	T > C	0.0072**
WT	:	G > A	0.0012***
WT	:	C > T	0.0003***
WT	:	O1O2m	< 0.0001***
T > C	:	G > A	0.7142
T > C	:	C > T	0.1874
T > C	:	O1O2m	0.0058**
G > A	:	C > T	0.7785
G > A	:	O1O2m	0.0396*
C > T	:	O1O2m	0.2238

fr.1 (3 Hp)			*P*-value
WT	:	T > C	0.0497*
WT	:	G > A	0.0007***
WT	:	C > T	0.0039***
WT	:	O1O2m	< 0.0001***
T > C	:	G > A	0.0909
T > C	:	C > T	0.4832
T > C	:	O1O2m	0.0004***
G > A	:	C > T	0.7413
G > A	:	O1O2m	0.0255*
C > T	:	O1O2m	0.0041***

C

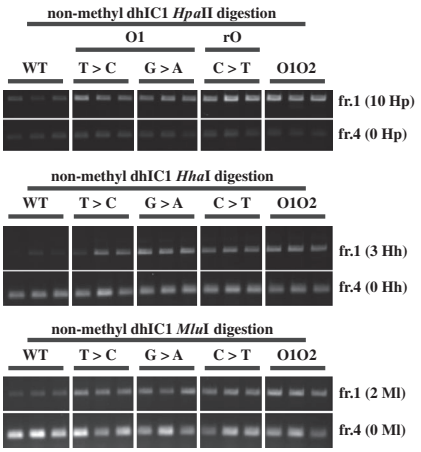

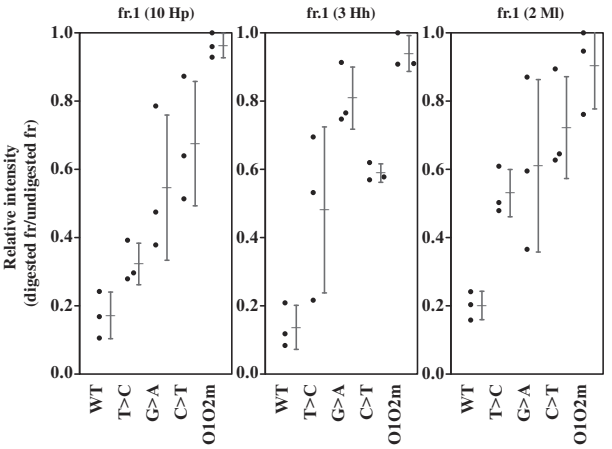

fr.1 (10 Hp)			*p*-value
WT	:	T > C	0.6469
WT	:	G > A	0.0389*
WT	:	C > T	0.0064**
WT	:	O1O2m	0.0002***
T > C	:	G > A	0.3057
T > C	:	C > T	0.0530
T > C	:	O1O2m	0.0011***
G > A	:	C > T	0.7569
G > A	:	O1O2m	0.0213*
C > T	:	O1O2m	0.1331

fr.1 (3 Hh)			*p*-value
WT	:	T > C	0.0397*
WT	:	G > A	0.0004***
WT	:	C > T	0.0077**
WT	:	O1O2m	0.0001***
T > C	:	G > A	0.0514
T > C	:	C > T	0.8136
T > C	:	O1O2m	0.0070**
G > A	:	C > T	0.2563
G > A	:	O1O2m	0.6936
C > T	:	O1O2m	0.0361*

fr.1 (2 MI)			*p*-value
WT	:	T > C	0.1168
WT	:	G > A	0.0419*
WT	:	C > T	0.0100 *
WT	:	O1O2m	0.0012***
T > C	:	G > A	0.9594
T > C	:	C > T	0.5304
T > C	:	O1O2m	0.0676
G > A	:	C > T	0.8785
G > A	:	O1O2m	0.1842
C > T	:	O1O2m	0.5851

A 21-bp deletion reported in BWS patients was associated with hIC1 hypermethylation [22]. Both the S2 and O2 motifs are deleted in this mutant hD1 element and it has a single nucleotide substitution in its O1 motif (Fig. S1A). We assumed that this microdeletion suppressed induction of hD1-dependent DNA demethylation. We examined the effects of the 21-bp deletion (21-del) and the O1 motif consensus mutation (T > A) on the induction of hD1-dependent DNA demethylation (Fig. S1A). The uhD1 with a 21-bp microdeletion did not induce DNA demethylation ($P = 0.0467$). The T > A mutant nonsignificantly repressed demethylation ($P = 0.0504$) (Fig. S1B). The S2 and O2 motifs are needed for the maximal induction of hD1-dependent DNA demethylation.

Oct motif variants in patients with BWS suppress DNA demethylation and cause the accumulation of methylated DNA on dhIC1

Our previous study showed that mouse SO motifs induce DNA demethylation and protect mIC1 from *de novo* methylation in P19 cells [10]. We postulated that hD1-dependent DNA demethylation maintains hIC1 in the unmethylated state and this defect causes aberrant hIC1 methylation.

We investigated the influence of hD1-dependent DNA demethylation on the methylation state of multiple CpG sites within hIC1 by cloning the downstream region of the 2.3-kb hIC1 element containing hD1, CBS4, CBS5, and CBS6 (dhIC1) and inserting BWS single nucleotide variants (T > C, G > A, or C > T) into the Gt(ROSA)26Sor locus *via* the Cre-lox system (Fig. 4A). Changes in dhIC1 methylation were assessed by MSRE-PCR using the ratio of bands of variable intensity (fr. 1–3) to those of invariable intensity (fr. 4) (Fig. 4A). Three primer sets were positioned to determine the inducible range of hD1-dependent demethylation (Fig. 4A).

When dhIC1s were methylated by *Hpa*II methyltransferase and introduced into Gt(ROSA)26Sor locus *in vitro*, there was a high level of DNA demethylation in the 2-kb WT dhIC1. Demethylation was significantly suppressed by the O1O2 mutation ($P = 0.0023$) (Fig. 4B; fr. 1). However, this activity declined in a manner dependent on the distance from hD1 (Fig. 4B, fr. 1 and fr. 3 of WT). The BWS single nucleotide variants T > C, G > A, and C > T tended to suppress demethylation in a 2-kb portion of dhIC1 (Fig. 4B, fr. 1). Based on the 1.5-kb and 1-kb PCR products of dhIC1, all three BWS variants reduced demethylation relative to WT (fr. 2: $P = 0.0072$, $P = 0.0012$, and $P = 0.0003$. fr. 3: $P = 0.0497$, $P = 0.0008$, and $P = 0.0039$, respectively). The dhIC1 with the Oct motifs may induce demethylation over ≥ 1682 bp from the hD1. All three BWS variants suppressed demethylation on dhIC1 but this effect was weaker than that for O1O2m (Fig. 4B).

We used transgenes without methyltransferase treatment to determine whether the failure of BWS variants to induce demethylation resulted in increased methylation in dhIC1. We noted that O1O2m dhIC1 substantially accumulated methylation, whereas WT dhIC1 remained relatively hypomethylated. All three BWS single nucleotide variants within the rO or O1 motifs accumulated methylation compared with WT dhIC1

Fig. 5. Oct motif variants in BWS patients inhibit the maintenance of the hypomethylated status of the CBS4 segment. (A) Map of the analyzed region using two methylation analysis methods. Top: Position of 19 CpG sites in the 300 bp region spanning from the vector sequence to the dhIC1-d56 region (shaded box). Square encompassing three CpG sites (CG15-CG17) indicates CBS4. Both CG8 and CG19 include *Hpa*II sites (H). Middle: Restriction map of the dhIC1-d56 region introduced onto the Gt(ROSA)26Sor locus. Black triangles indicate hybrid lox sites formed by recombination between lox66 and lox71. Open circle and rhombus indicate CBS4 and Sox-Oct motifs (hD1), respectively. *Hpa*II (H) and *Hha*I (Hh) sites are shown. Bottom: Fragments amplified by PCR for MESR-PCR and bisulfite sequencing. Two fragments (fr. 1–2) were amplified depending on the methylation level of the restriction sites. Fr. 3 was amplified to correct the quantity of template DNA. Primers are indicated by arrows. The number of restriction sites in amplified fragments for MSRE-PCR is shown on the right. Position of primer sets for nested PCR used in the bisulfite sequence method is shown (Bisulfite-Seq). (B) Estimation of dhIC1-d56 methylation change in BWS variants. Left: amplified fragments from *Hpa*II- or *Hha*I-digested WT and mutant dhIC1-d56 regions. Right: methylation status of initially methylated *Hpa*II sites and initially unmethylated *Hha*I sites on WT and mutant dhIC1-d56 regions. Results of three biological replicates are shown. Data were analyzed using Tukey's HSD test. ***$P < 0.005$, **$P < 0.01$, *$P < 0.05$. Error bars represent standard deviation (SD). *P*-values are listed right side of the plot. One of the biological replicates using for bisulfite sequencing and direct bisulfite sequencing is shown as black triangles. (C) Estimation of dhIC1 *de novo* methylation in BWS variants. Left: amplified fragments from *Hpa*II- or *Hha*I-digested WT and mutant dhIC1-d56 regions. Right: methylation level of initially unmethylated restriction sites on the WT and mutant dhIC1-d56 regions. Results of three biological replicates are shown. Data were analyzed using Tukey's HSD test. ***$P < 0.005$, **$P < 0.01$, *$P < 0.05$. Error bars represent standard deviation (SD). *P*-values are listed right side of the plot. (D) Methylation analysis of 19 CpG sites in initially *Hpa*II methylated transgenes with bisulfite sequencing. The open and filled circles indicate unmethylated and methylated CpG molecules, respectively. Each horizontal line represents a single clone.

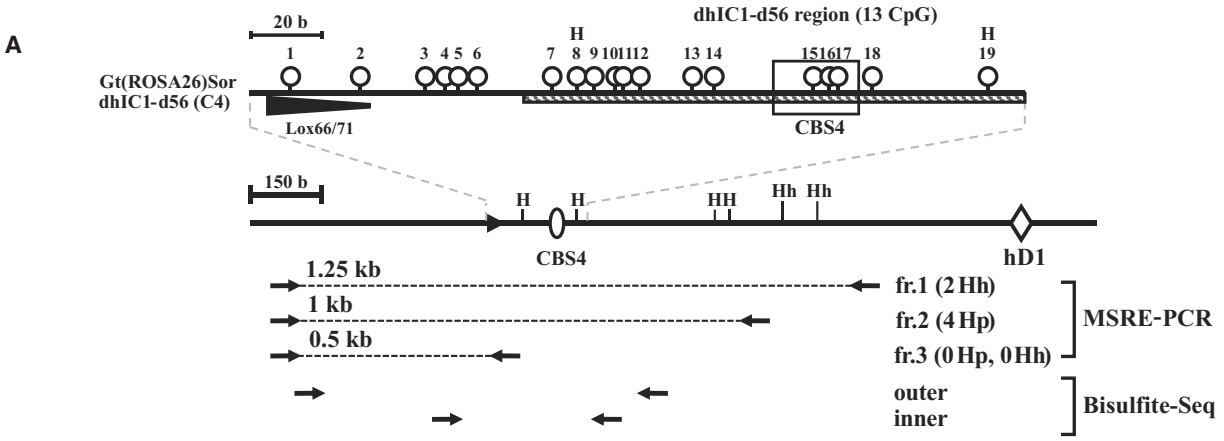

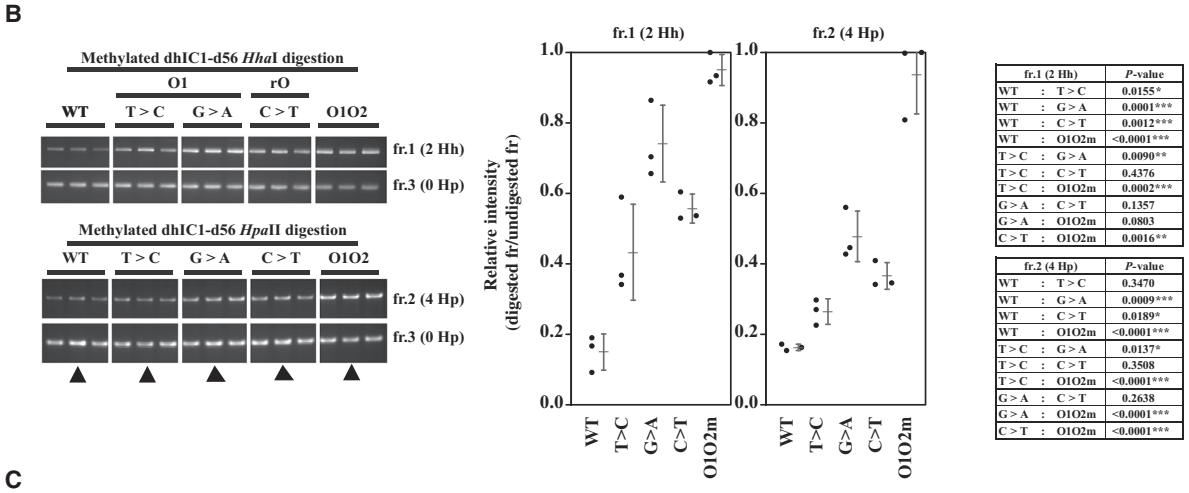

fr.1 (2 Hh)	*P*-value
WT : T > C	0.0155*
WT : G > A	0.0001***
WT : C > T	0.0012**
WT : O1O2m	<0.0001***
T > C : G > A	0.0090**
T > C : C > T	0.4376
T > C : O1O2m	0.0002***
G > A : C > T	0.1357
G > A : O1O2m	0.0803
C > T : O1O2m	0.0016**

fr.2 (4 Hp)	*P*-value
WT : T > C	0.3470
WT : G > A	0.0009***
WT : C > T	0.0189*
WT : O1O2m	<0.0001***
T > C : G > A	0.0137*
T > C : C > T	0.3508
T > C : O1O2m	<0.0001***
G > A : C > T	0.2638
G > A : O1O2m	<0.0001***
C > T : O1O2m	<0.0001***

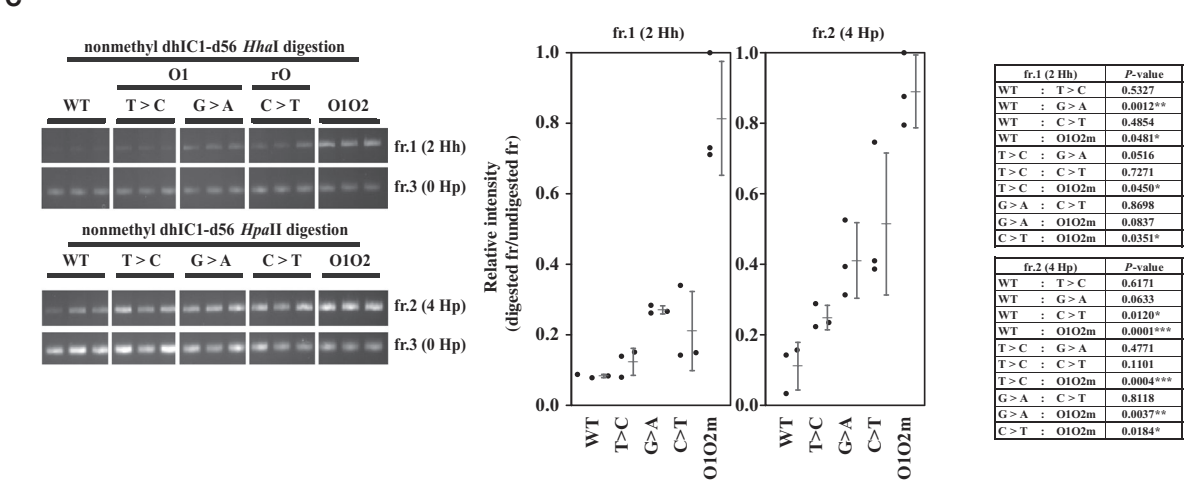

fr.1 (2 Hh)	*P*-value
WT : T > C	0.5327
WT : G > A	0.0012**
WT : C > T	0.4854
WT : O1O2m	0.0481*
T > C : G > A	0.0516
T > C : C > T	0.7271
T > C : O1O2m	0.0450*
G > A : C > T	0.8698
G > A : O1O2m	0.0837
C > T : O1O2m	0.0351*

fr.2 (4 Hp)	*P*-value
WT : T > C	0.6171
WT : G > A	0.0633
WT : C > T	0.0120*
WT : O1O2m	0.0001***
T > C : G > A	0.4771
T > C : C > T	0.1101
T > C : O1O2m	0.0004***
G > A : C > T	0.8118
G > A : O1O2m	0.0037**
C > T : O1O2m	0.0184*

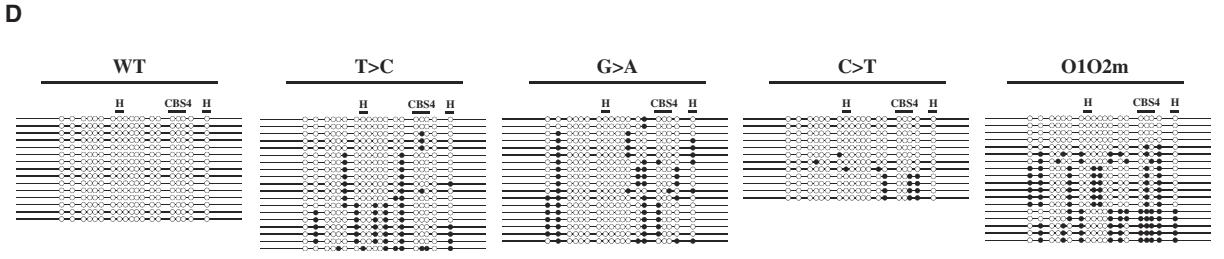

(Hp: $P = 0.6469$, $P = 0.0389$, and $P = 0.0064$. Hh: $P = 0.0397$, $P = 0.0004$, and $P = 0.0077$. Ml: $P = 0.1168$, $P = 0.0419$, and $P = 0.0101$, respectively) (Fig. 4C).

We investigated the methylation levels of the CBS4-encompassing region using two methods with sodium bisulfite-treated DNA; sequencing analysis of cloned PCR-amplified fragments and direct sequencing analysis of PCR-amplified fragments, to determine whether the methylation levels of CpGs overlap with restriction sites. Because the CBS4 region was not stably amplified from the Gt(ROSA)26Sor locus-integrated 2.3 kb dhIC1 fragment, we used the 1.3 kb dhIC1 fragment containing the hD1 and CBS4 regions (dhIC1-d56) obtained by deleting the CBS5 and CBS6 regions from the 2.3 kb dIC1 fragment (Fig. 5A). We first estimated the effect of variants on the methylation status at *Hpa*II and *Hha*I sites using the MESR-PCR method (Fig. 5B,C).

In *Hpa*II methyltransferase pretreated dhIC1, a 1-kb PCR product showed the significant suppression of DNA demethylation in O1O2m (fr. 2: $P < 0.0001$). BWS variants tended to suppress demethylation, even though the degree was weak in T > C (fr. 2: $P = 0.3470$, $P = 0.0009$, and $P = 0.0189$). In contrast, three BWS variants showed a significant increase in DNA methylation at *Hha*I sites (fr. 1: $P = 0.0155$, $P = 0.001$, and $P = 0.0012$) (Fig. 5B). Transgenes without *Hpa*II methyltransferase treatment tended to accumulate DNA methylation in the presence of three BWS variants (fr. 1: $P = 0.5327$, $P = 0.0012$, and $P = 0.4854$; fr. 2: $P = 0.6171$, $P = 0.0633$, and $P = 0.0120$, respectively) (Fig. 5C).

Using the bisulfite sequencing method, we analyzed the methylation status of 19 CpGs of cloned fragments amplified from one of the biological replicates shown in Fig. 5B (Fig. 5D). Two premethylated *Hpa*II sites (CG8 and CG19) and CBS4 are contained in 13 CpGs located within the dhIC1-d56 region. We observed suppression of DNA demethylation in CG19 in T > C and G > A variants and O1O2m but not in WT and C > T variants. The CG8 of all transfectants were highly demethylated. The difference in demethylation was also detected with direct bisulfite sequence (Fig. S2). Methylation levels of CpG sites were markedly increased in O1O2m dhIC1-d56, whereas no methylation accumulation was observed in WT. Three BWS mutations showed an increase in DNA methylation. In addition, changes in methylation status depending on the presence of the three BWS variants were accompanied by the acquisition of DNA methylation within the CBS4 (Fig. 5D).

Discussion

In this study, the 247-bp hD1 element derived from human IC1 induced DNA demethylation in the plasmids and nuclei of P19 cells. Using a stable transfection-based assay, we previously showed that the 74-bp hD1 element induces DNA demethylation in P19 cells [13]. Nevertheless, this effect was unclear as the element randomly integrated into the genome may be affected by the surrounding chromatin structure. Moreover, the 74-bp hD1 element may not suffice to induce DNA demethylation toward the distal site. Unlike the present study, in previous experiments, the hD1 elements did not include the upstream or downstream regions. It was also determined from the distal test fragment (~ 200 bp) whether demethylation occurred at *Hpa*II sites [10]. In the present study, we applied a transient transfection-based assay to estimate hD1-dependent demethylation. This assay quantifies sequence-specific DNA demethylation at the *Hpa*II site 5 bp distant from the test fragment. The latter is a singular detectable demethylation site [13]. We cloned dhD1 and uhD1 and consistently detected DNA demethylation by transient transfection-based assay. Mutations of the two Oct motifs in hD1 strongly inhibited demethylation. We concluded that the hD1 element with flanking region demethylates DNA and that Oct motifs play a pivotal role in this process in P19 cells.

The SO motifs and the CBS in mIC1 maintain the hypomethylated state. We previously showed that in P19 cells, Oct motif-dependent DNA demethylation is induced in mIC1 within ≥ 1 kb from the SO motifs and protects mIC1 from *de novo* DNA methylation [10]. In mice, the mutation or deletion of SO motifs upregulated DNA methylation on maternal mIC1 after implantation [11,12]. CBS is required for the induction of DNA demethylation in undifferentiated cell lines [11,29] and the maintenance of the unmethylated state in mIC1 during mouse development [7,8]. To date, however, there is no direct evidence that the CBSs or Oct motifs maintain hIC1 in a hypomethylated state. Recently, the sequences required to maintain hIC1 in a hypomethylated state were elucidated using a mouse model. Substitution of the mIC1 with human IC1 maintained maternally inherited hypomethylation following mouse embryogenesis [30].

The recombined human IC1 with 2.2-kb region deletion containing three CBSs (CBS3, CBS4, and CBS5) and hD1 increased methylation at CBS1 and CBS6 [31]. These reports suggested that the deleted region contains functional sequences required to maintain hIC1 hypomethylation.

We have examined the effects of three variants of Oct motifs in the hD1 region on the induction of DNA demethylation in transiently transfected plasmids and the hypomethylation maintenance ability on fragments from hIC1 integrated into genomic DNA. These three variants were found in patients with BWS who have maternal hIC1 hypermethylation [19–23]. T > C and G > A variants are located in the O1 motif, and a C > T mutation is located in the rO motif (Fig. 1A). The onset of BWS was observed in patients who carried these variants due to the maternal inheritance but not paternal inheritance. These variants of the Oct motif(s) disrupt hD1-dependent DNA demethylation and cause the accumulation of methylation in dhIC1 containing CBS4, CBS5, and CBS6 (Fig. 4). In addition, bisulfite sequencing revealed that the accumulation of methylation was promoted by three variants found in BWS patients (Fig. 5). Therefore, the Oct motifs in hD1 probably maintain hIC1 DNA in a hypomethylated state to prevent an increase in methylation after implantation.

The results of bisulfite sequencing and direct bisulfite sequencing showed that the inhibition of CG19 demethylation depends on the presence of sequence variations in the Oct motifs, even though the degree was varied (Fig. 5 and Fig. S2). These results indicated that hD1-dependent DNA demethylation is involved in the regulation of methylation levels of CG19. High levels of CG8 demethylation were detected even in the O1O2m dhIC1, with both bisulfite sequencing and direct bisulfite sequencing methods, suggesting that CG8 is demethylated in an hD1-independent manner. These methylation levels of CG8 were inconsistent with the degree of PCR amplification after *Hpa*II digestion (MSRE-PCR, Fig. 5B,C). We speculate that low-level DNA methylation of CG8 occurred and that the levels of methylation depend on variant-specific effects. In this study, methylation levels of CpGs do not overlap with restriction sites were analyzed only in the CBS4 region. However, because methylation levels in dhIC1 and dhIC1-d56, estimated with MSRE-PCR, were similar at both premethylated and unmodified sites, it is suggested that CpGs widely distributed in the dhIC1 region are protected from increased methylation *via* Oct motif-dependent hypomethylation maintenance mechanisms such as the induction of demethylation activity.

We showed that BWS variants tightly suppressed Oct motif-dependent DNA demethylation at the hD1 element of the proximal *Hpa*II site on plasmids (Fig. 3). On dhIC1 and dhIC1-d56 with a BWS variant selectively integrated into the genomic DNA, distinct demethylation levels were observed at the *Hpa*II sites at ~ 1 kb distant from the SO motifs (Fig. 4 and Fig. 5). Thus, the slight Oct motif-dependent DNA demethylation retained by the hD1-containing region could be enhanced by histone modification of the transgenes on the chromosome. Histone modification is associated with epigenetic regulation and DNA methylation. Histone methylation or acetylation such as H3K4me3, H3K4me3, and H3K9ac increases open chromatin. H3K4me3 is associated with the transition from 5mC to 5hmC in the TET demethylase pathway [32]. Aberrant DNA methylation in maternal hIC1 decreases H3K4me2 and H3K9ac and increases H3K9me3 and H3K27me3. These processes comprise the repressive modification associated with closed chromatin formation [6]. The relationship between the Oct motifs within hIC1 and histone modification is unknown. Nevertheless, our results suggest that Oct motif-dependent demethylation may regulate histone modification, enhance demethylation, and maintain IC1 hypomethylation.

The Oct motifs significantly influence hD1-dependent demethylation. Consensus disruption of the O1 motif or single nucleotide substitutions of the O1 or rO motifs markedly suppressed demethylation. In contrast, consensus disruption of the S1, S2, and O2 motifs had little or no effect on demethylation. Several single nucleotide substitutions in hD1 were detected in BWS patients and were accompanied by hIC1 hypermethylation [19–23]. To date, however, there is no published report describing single nucleotide variant in the S1, S2, or O2 motifs. For single nucleotide substitutions in hD1, BWS hypermethylation is associated with the lack of Oct motif-dependent DNA demethylation.

The findings of the present study suggest that the levels of DNA demethylation induced with the hD1 element *in vitro* explain the association between BWS variants in hD1 and the accumulation of methylation observed in BWS patients. However, it remains unknown how hD1-dependent DNA demethylation occurs or spreads within the hIC1. Analysis of other BWS variants outside of hD1 will help to understand the molecular mechanisms. In addition, it is unclear whether hD1-dependent DNA demethylation is involved in the initiation of inherited methylation status in germ cells.

Thus, further studies on the influence of variants on hIC1 methylation using a mutant hIC1-bearing mouse model in addition to *in vitro* studies to elucidate the genetic cause of hIC1 hypermethylation in BWS patients are needed.

Materials and methods

Plasmid construction and *in vitro* methylation

To examine the induction of demethylation, an oligo DNA fragment was inserted into the *Hind*III site of pEdBS1 to form pEdBS2 [10]. The sequence of the fragment was 5′-AGC TGT ACC CAA AGA CCG GTC GAC ATC GAT AGA TCT AAG CTT CTG CAG GAA TTC GAT-3′. Human DNA fragments from IC1 were amplified by PCR from human embryonic kidney 293 (HEK293) cell genomic DNA. The dhD1 and uhD1 fragments with or without sequence variant were amplified using the primers listed in Table S2. Fragments with sequence variants (variations) (O1O2m, C > T, T > C, G > A, and T > A) were generated by ligating two fragments amplified with the primer set listed in Table S2. The sticky ends of the amplified fragments were connected by digestion with *Bsa*I whose recognition site was located in the primer. Fragments with consensus variants (S1, O1, S2, and O2) were generated by ligating synthesized oligonucleotides (Table S3). O2 was disrupted by a two-nucleotide substitution that was also used to disrupt the Oct motifs in mIC1 (Fig. 2). The nucleotide substitutions in the Oct motifs of mIC1 suppress OCT3/4 protein binding to the mouse Oct motifs [13]. O1 was disrupted by the same and another pair of nucleotide substitution. S1 and S2 were disrupted by the substitution of three nucleotides. Nucleotide substitutions at the same positions in the Sox motif of mIC1 suppressed SOX2 protein binding to the mouse Sox motifs [13].

To determine the dhIC1 methylation status with and without the sequence variants at the gt(ROSA26)Sor locus, each ICR fragment was inserted into the pL71 vector. The latter was a pEGFP-N3-based plasmid with a neomycin resistance gene and was prepared as follows. Multicloning sites (MCS) between *Bgl*II and *BamH*I were removed and ligated. The MCS from pBluescript II (*BssH*II–*BssH*II) was inserted into the blunted *Ase*I site. A lox71 fragment was generated by annealing the synthetic oligonucleotides 5′-CTA CCG TTC GTA TAG CAT ACA TTA TAC GAA GTT ATG GGC C-3′ (lox71 upper) and 5′-CAT AAC TTC GTA TAA TGT ATG CTA TAC GAA CGG TAG GTA C-3′ (lox71 lower) and was inserted into the *Kpn*I-*Apa*I site (pL71) [33]. dhIC1 is a 2.3 kb DNA fragment (hg19, chr11; 2 020 912–2 023 184) flanked by the *Xho*I and *Hin*dIII sites. dhIC1-d56 is a 1.3 kb DNA fragment (hg19, chr11; 2 021 932–2 023 184) flanked by the blunted *Hae*II and *Hin*dIII sites. The DNA sequence of the 2.3-kb fragment contains one of two HG00096 haplotypes in a 1000-genome database and differs by 10 nt from the hg19 sequence. The latter is the major haplotype of the amplified portion in 5008 alleles of the database. The dhIC1 fragment with a BWS variant was generated by replacing the internal *Sal*I-*Cla*I fragment with those bearing each of the BWS variants (C > T, T > C, and T > A). To test the regulation of the hypomethylated state in the genome, dhIC1 fragments with or without sequence variations were inserted into the pL71 vector (pL71-dhIC1). The vector included the lox71 sequence for Cre-mediated recombination with the lox66 sequence at the gt(ROSA26)Sor locus in P19-ROSA-L66 cells [33]. dhIC1-d56 is a 1.3 kb DNA fragment excised from pL71-dhIC1 with *Hae*II and *Xba*I sites and inserted into the *Eco*RV-*Xba*I sites of the pL71 vector (pL71-dhIC1).

The constructs used in the demethylation assays were methylated *in vitro* with bacterial *Hpa*II methyltransferase (M.*Hpa*II; New England Biolabs, Ipswich, MA, USA). Prior to transfection, methylation was confirmed by digestion with 8–10 units of *Hpa*II restriction endonucleases per microgram methylated plasmid. The plasmids that were completely methylated at the *Hpa*II sites were used in the subsequent transfection experiments.

Cloning of P19-Rosa-L66 cells

The lox66 element was inserted into the Gt (ROSA)26Sor intron 1 (mm9, chr6: between 113 025 351 and 113 025 352) of P19 cells by homologous recombination after digestion with pX330-U6-Chimeric_BB-CBh-hSpCas9 (No. 42230; Addgene, Watertown, MA, USA). A plasmid was constructed that bore a 353-bp Gt (ROSA)26Sor intron 1 sequence upstream of the insertion site, a lox66 sequence, a puromycin resistance gene with the SV40 bracketed by FAS loxP2 sequences, and a downstream 384-bp sequence from the insertion site (pL66). The primers are listed in Table S4. The lox66 and two FAS loxP2 fragments were generated by annealing the synthetic oligonucleotides 5′-AGC TTA TAA CTT CGT ATA GCA TAC AT TAT ACG AAC GGT AGA T-3′ (lox66 upper), 5′-ATC TAC CGT TCG TAT AAT GTA TGC TAT ACG AAG TTA TA-3′ (lox66 lower), 5′-AAT TCA TAA CTT CGT ATA TAC CTT TCT ATA CGA AGT TAT CTG CA-3′ (FAS loxP2 #1 upper), 5′- GAT AAC TTC GTA TAG AAA GGT ATA TAC GAA GTT ATG-3′ (FAS loxP2 #1 lower), 5′-GAT CCA TAA CTT CGT ATA TAC CTT TCT ATA CGA AGT TAT A-3′ (FAS loxP2 #2 upper), and 5′- CTA GTA TAA CTT CGT ATA GAA AGG TAT ATA CGA AGT TAT G-3′ (FAS loxP2 #2 lower). FAS loxP2 contains a C to T transition at position 2 and a G to A transition at position 33 of FAS loxP sequence [34]. Recombinant P19 cells were selected by incubation with 1 $\mu g \cdot mL^{-1}$ puromycin for 24 h then isolated as single cells. After 20 days, one clonal P19 cell carrying a lox66 sequence at intron 1 of Gt (ROSA)26Sor was selected (P19-ROSA-L66 cell).

Cell culture and transfection

The mouse embryonic carcinoma cell lines P19 and P19-ROSA-L66 were maintained in an alpha modification of Eagle's medium supplemented with 5% (w/v) heat-inactivated fetal bovine serum (FBS), 5% (w/v) heat-inactivated

bovine calf serum (BCS), and 0.2% (w/v) penicillin/streptomycin sulfate. P19 and P19-ROSA-L66 cells were replated at a density of 0.5×10^5 in a 3.5-cm dish 24 h before transfection. P19 cells were transfected with 1.5 μg pEd-BSII methylated *in vitro* by *Hpa*II. Transfected cells were harvested after 72 h and used in Southern blot analysis. P19-ROSA-L66 cells were cotransfected with pL71-dhIC1 or pL71-dhIC1-d56 either unmethylated or methylated *in vitro* and the Cre expression vector pCAG-Cre (No. 13775; Addgene) at a 5 : 1 ratio. Transfected cells were selected by incubation with 600 μg mL^{-1} neomycin for 14 days. Genomic DNA from the polyclonal cells in the culture dish was extracted and used in MSRE-PCR and bisulfite sequencing.

Southern blot analysis

Five micrograms of total DNA harvested from transfected P19 cells was digested with *Sac*I (TOYOBO, Osaka, Japan) and methylation-sensitive *Hpa*II (Thermo Fisher Scientific, Waltham, MA, USA). The DNA digests were electrophoresed on 1.3% (w/v) agarose gel, transferred to nylon membranes (Hybond-XL™; GE Healthcare, Little Chalfont, UK), and used for hybridization. Probes were radiolabeled with a BcaBEST labeling kit (Takara Bio Inc., Kusatsu, Shiga, Japan) and hybridized to a membrane in 6× SSPE 1× Denhardt's solution, 0.5% (w/v) SDS, and 200 μg·mL^{-1} salmon sperm DNA at 64 °C over two nights. After hybridization, the membranes were sequentially washed in 2× SSPE–0.1% (w/v) SDS at 20–25 °C, 0.2× SSPE–0.1% (w/v) SDS at 20–25 °C, and 0.2× SSPE–0.1% (w/v) SDS at 64 °C. Hybridized filters were subjected to autoradiography and quantified with a BAS-2500 Bio Imaging Analyzer (Fujifilm, Tokyo, Japan). DNA demethylation was calculated as follows: the radioactive count of a band generated by digestion at the *Hpa*II site (fr. 3) was divided by the total radioactive count for all bands (fr. 1–6).

Methylation-sensitive restriction enzyme (MSRE) PCR analysis

Two micrograms of total DNA harvested from transfected P19-ROSA-L66 was digested with methylation-sensitive *Hpa*II (Thermo Fisher Scientific), *Hha*I (TaKaRa Bio Inc.), or *Mlu*I (TaKaRa Bio Inc.). The DNA digests were tuned to 100 ng μL^{-1} after purification with a phenol/chloroform mixture and ethanol. The target portion was amplified from 100 ng digested DNA using Tks Gflex™ DNA polymerase (TaKaRa Bio Inc.) in 10 μL total volume. The primers used in the reactions were as follows: forward primer for all fragments of dhIC1 (fr. 1–4) and dhIC1-d56 (fr. 1-3), 5′-GTA TTT TCC ATC GAG GTA GAT TAA AGA C-3′; reverse primer for dhIC1 fr. 1 and dhIC1-d56 fr. 2, 5′-GAA TCA GTT GAA GGT ATG GAA AC-3′; reverse primer for dhIC1 fr. 2, 5′-ACA ATG AAG TGT CCC CAT TCT T-3′; reverse primer for dhIC1 fr. 3, 5′-GAG GAG ATA CTA GGG GAA CAA TGA G-3′; reverse primer for dhIC1 fr. 4, 5′-GAC TCA AGT CAC GCC TAC TTA TGT GAT GAT-3′; reverse primer for dhIC1-d56 fr. 1, 5′-CAC TGA AGC TGG GAC AGG AGA GCA GA-3′; reverse primer for dhIC1-d56 fr. 3 5′-AAG CTT ATC GAT ACC GTC GAC CTC-3′. Two microliters of amplified fragment 1, 2, or 3 was mixed with 2 μL fragment 4 and electrophoresed on 1.3% (w/v) agarose gels. The electrophoresed gels were stained with ethidium bromide, photographed, and saved as TIFF image files with Printgraph AE-6914 (ATTO Technology, Amherst, NY, USA). Band intensities were quantified with Multi Gauge (v. 3.1; Fujifilm). Band intensities of the fragments were normalized with those of fr. 4 and corrected such that the highest band intensity in each set of amplified fragments was 1.0.

Bisulfite sequencing

Genomic DNA extracted from P19-ROSA-L66 cells were treated with sodium bisulfite using EZ DNA methylation-gold kit (ZYMO RESEARCH Inc., Irvine, CA, USA). A total of 200 ng of bisulfite-converted DNA was used as a template for nested PCR amplification with Epi-Taq HS DNA polymerase (TaKaRa Bio Inc.) using two sets of primers: outer primer forward, 5′-TTT TTT GTT TGA GAT TTT TAT TAT AGT ATG-3′; outer primer reverse, 5′-AAA AAA CAA TAA AAT ATC CCC ATT CTT-3′; inner primer forward, 5′-GGT TGT AGT TGG GGT TTT AAT ATT GTA-3′ and inner primer reverse 5′-CTC CCA CAA AAT CTC TAA CAA ACT C-3′. Amplified PCR products were subcloned into the T-vector pMD20 (TaKaRa Bio Inc.) or directly sequenced. Sequencing was performed using a DNA sequencing service (Macrogen, Kyoto, Japan) with primers 5′-GTT TTC CCA GTC ACG AC-3′ (cloned plasmids) or 5′-GGT TGT AGT TGG GGT TTT AAT ATT GTA-3′ (PCR fragments). Sequencing data were analyzed with QUMA (http://quma.cdb.riken.jp/) [35].

Statistical analysis

Bartlett's test was used to determine the multiple test methods required for the data. Tukey's HSD or Games-Howell's test was performed in the event of a null hypothesis for Bartlett's test when $P = 0.05$ was not rejected or rejected, respectively. 'R' version 3.4.4 (The R Foundation for Statistical Computing, Vienna, Austria) was used for all analyses.

Acknowledgements

We are grateful to Dr. Keiji Tanimoto of the University of Tsukuba for helpful discussions. We thank

Tomoya Takahashi and all members of our laboratory for their invaluable contributions. We also thank Editage (http://www.editage.com) for English language editing.

Author contributions

SK, NH and KH conceived the study. SK, NH, KH and CS designed the experiments. NH, KH and CS supervised the study. SK, CM, HO and TS performed experiments. SK, NH and CM analyzed data. SK and NH wrote the manuscript and made manuscript revisions.

References

1 Edwards CA and Ferguson-Smith AC (2007) Mechanisms regulating imprinted genes in clusters. *Curr Opin Cell Biol* **19**, 281–289.
2 Ishida M and Moore GE (2013) The role of imprinted genes in humans. *Mol Aspects Med* **34**, 826–840.
3 Barlow DP and Bartolomei MS (2014) Genomic Imprinting in Mammals. *Cold Spring Harb Perspect Biol* **6**, a018382.
4 Bell AC and Felsenfeld G (2000) Methylation of a CTCF-dependent boundary controls imprinted expression of the Igf2 gene. *Nature* **405**, 482–485.
5 Hark AT, Schoenherr CJ, Katz DJ, Ingram RS, Levorse JM and Tilghman SM (2000) CTCF mediates methylation-sensitive enhancer-blocking activity at the H19/Igf2 locus. *Nature* **405**, 486–489.
6 Nativio R, Sparago A, Ito Y, Weksberg R, Riccio A and Murrell A (2011) Disruption of genomic neighbourhood at the imprinted IGF2-H19 locus in Beckwith-Wiedemann syndrome and Silver-Russell syndrome. *Hum Mol Genet* **20**, 1363–1374.
7 Schoenherr CJ, Levorse JM and Tilghman SM (2003) CTCF maintains differential methylation at the Igf2/H19 locus. *Nat Genet* **33**, 66–69.
8 Engel N, Thorvaldsen JL and Bartolomei MS (2006) CTCF binding sites promote transcription initiation and prevent DNA methylation on the maternal allele at the imprinted H19/Igf2 locus. *Hum Mol Genet* **15**, 2945–2954.
9 Ibala-Romdhane S, Al-Khtib M, Khoueiry R, Blachère T, Guérin J-F and Lefèvre A (2011) Analysis of H19 methylation in control and abnormal human embryos, sperm and oocytes. *Eur J Hum Genet* **19**, 1138–1143.
10 Hori N, Nakano H, Takeuchi T, Kato H, Hamaguchi S, Oshimura M and Sato K (2002) A Dyad Oct-binding sequence functions as a maintenance sequence for the unmethylated state within the H19 / Igf2 -imprinted control region. *J Biol Chem* **277**, 27960–27967.
11 Zimmerman DL, Boddy CS and Schoenherr CS (2013) Oct4/Sox2 binding sites contribute to maintaining hypomethylation of the maternal Igf2/H19 imprinting control region. *PLoS ONE* **8**, e81962.
12 Sakaguchi R, Okamura E, Matsuzaki H, Fukamizu A and Tanimoto K (2013) Sox-Oct motifs contribute to maintenance of the unmethylated H19 ICR in YAC transgenic mice. *Hum Mol Genet* **22**, 4627–4637.
13 Hori N, Yamane M, Kouno K and Sato K (2012) Induction of DNA demethylation depending on two sets of Sox2 and adjacent Oct3/4 binding sites (Sox-Oct motifs) within the mouse H19 /insulin-like growth factor 2 (Igf2) imprinted control region. *J Biol Chem* **287**, 44006–44016.
14 Weksberg R, Shuman C and Beckwith JB (2010) Beckwith-Wiedemann syndrome. *Eur J Hum Genet* **18**, 8–14.
15 Kalish JM, Jiang C and Bartolomei MS (2014) Epigenetics and imprinting in human disease. *Int J Dev Biol* **58**, 291–298.
16 Bliek J (2001) Increased tumour risk for BWS patients correlates with aberrant H19 and not KCNQ1OT1 methylation: occurrence of KCNQ1OT1 hypomethylation in familial cases of BWS. *Hum Mol Genet* **10**, 467–476.
17 Cooper WN, Luharia A, Evans GA, Raza H, Haire AC, Grundy R, Bowdin SC, Riccio A, Sebastio G, Bliek J *et al.* (2005) Molecular subtypes and phenotypic expression of Beckwith-Wiedemann syndrome. *Eur J Hum Genet* **13**, 1025–1032.
18 Cerrato F, Sparago A, Verde G, De Crescenzo A, Citro V, Cubellis MV, Rinaldi MM, Boccuto L, Neri G, Magnani C *et al.* (2008) Different mechanisms cause imprinting defects at the IGF2/H19 locus in Beckwith-Wiedemann syndrome and Wilms' tumour. *Hum Mol Genet* **17**, 1427–1435.
19 Demars J, Shmela ME, Rossignol S, Okabe J, Netchine I, Azzi S, Cabrol S, Le Caignec C, David A, Le Bouc Y *et al.* (2010) Analysis of the IGF2/H19 imprinting control region uncovers new genetic defects, including mutations of OCT-binding sequences, in patients with 11p15 fetal growth disorders. *Hum Mol Genet* **19**, 803–814.
20 Berland S, Appelbäck M, Bruland O, Beygo J, Buiting K, Mackay DJ, Karen Temple I and Houge G (2013) Evidence for anticipation in Beckwith-Wiedemann syndrome. *Eur J Hum Genet* **21**, 1344–1348.
21 Higashimoto K, Jozaki K, Kosho T, Matsubara K, Fuke T, Yamada D, Yatsuki H, Maeda T, Ohtsuka Y, Nishioka K *et al.* (2014) A novel de novo point mutation of the OCT-binding site in the IGF2 / H19 -imprinting control region in a Beckwith-Wiedemann syndrome patient: a novel mutation of the OCT-binding site in BWS. *Clin Genet* **86**, 539–544.

22 Abi Habib W, Azzi S, Brioude F, Steunou V, Thibaud N, Das Neves C, Le Jule M, Chantot-Bastaraud S, Keren B, Lyonnet S *et al.* (2014) Extensive investigation of the IGF2/H19 imprinting control region reveals novel OCT4/SOX2 binding site defects associated with specific methylation patterns in Beckwith-Wiedemann syndrome. *Hum Mol Genet* **23**, 5763–5773.
23 Poole RL, Leith DJ, Docherty LE, Shmela ME, Gicquel C, Splitt M, Temple IK and Mackay DJ (2012) Beckwith-Wiedemann syndrome caused by maternally inherited mutation of an OCT-binding motif in the IGF2/H19-imprinting control region, ICR1. *Eur J Hum Genet* **20**, 240–243.
24 Higashimoto K, Nakabayashi K, Yatsuki H, Yoshinaga H, Jozaki K, Okada J, Watanabe Y, Aoki A, Shiozaki A, Saito S *et al.* (2012) Aberrant methylation of H19-DMR acquired after implantation was dissimilar in soma versus placenta of patients with Beckwith-Wiedemann syndrome. *Am J Med Genet* **158A**, 1670–1675.
25 Khan A, Fornes O, Stigliani A, Gheorghe M, Castro-Mondragon JA, van der Lee R, Bessy A, Chèneby J, Kulkarni SR, Tan G *et al.* (2018) JASPAR 2018: update of the open-access database of transcription factor binding profiles and its web framework. *Nucleic Acids Res* **46**, D260–D266.
26 Chew JL, Loh YH, Zhang W, Chen X, Tam WL, Yeap LS, Li P, Ang YS, Lim B, Robson P *et al.* (2005) Reciprocal transcriptional regulation of Pou5f1 and Sox2 via the Oct4/Sox2 complex in embryonic stem cells. *Mol Cell Biol* **25**, 6031–6046.
27 Rodda DJ, Chew JL, Lim LH, Loh YH, Wang B, Ng HH and Robson P (2005) Transcriptional regulation of Nanog by OCT4 and SOX2. *J Biol Chem* **280**, 24731–24737.
28 Onuchic V, Lurie E, Carrero I, Pawliczek P, Patel RY, Rozowsky J, Galeev T, Huang Z, Altshuler RC, Zhang Z *et al.* (2018) Allele-specific epigenome maps reveal sequence-dependent stochastic switching at regulatory loci. *Science* **361**, eaar3146.
29 Rand E, Ben-Porath I, Keshet I and Cedar H (2004) CTCF elements direct allele-specific undermethylation at the imprinted H19 locus. *Curr Biol* **14**, 1007–1012.
30 Ideraabdullah FY, Thorvaldsen JL, Myers JA and Bartolomei MS (2014) Tissue-specific insulator function at H19/Igf2 revealed by deletions at the imprinting control region. *Hum Mol Genet* **23**, 6246–6259.
31 Freschi A, Hur SK, Valente FM, Ideraabdullah FY, Sparago A, Gentile MT, Oneglia A, Di Nucci D, Colucci-D'Amato L, Thorvaldsen JL *et al.* (2018) Tissue-specific and mosaic imprinting defects underlie opposite congenital growth disorders in mice. *PLoS Genet* **14**, e1007243.
32 Kubiura M, Okano M, Kimura H, Kawamura F and Tada M (2012) Chromosome-wide regulation of euchromatin-specific 5mC to 5hmC conversion in mouse ES cells and female human somatic cells. *Chromosome Res* **20**, 837–848.
33 Albert H, Dale EC, Lee E and Ow DW (1995) Site-specific integration of DNA into wild-type and mutant lox sites. *Plant J* **7**, 649–659.
34 Siegel RW, Jain R and Bradbury A (2001) Using an in vivo phagemid system to identify non-compatible loxP sequences. *FEBS Lett* **505**, 467–473.
35 Kumaki Y, Oda M and Okano M (2008) QUMA: quantification tool for methylation analysis. *Nucleic Acids Res* **36**, W170–W175.

Supporting information

Additional supporting information may be found online in the Supporting Information section at the end of the article.

Fig. S1. Deletion of 21-bp region comprising the S2 and O2 motifs and reducing demethylation in BWS patients.

Fig. S2. Methylation analysis of 19 CpG sites using direct bisulfite sequencing.

Table S1. JASPR scores and relative scores of the Sox-Oct motif-like motifs within the human and mouse H19-ICR.

Table S2. Primers used for PCR amplification of dhD1 and uhD1 fragments with or without sequence variant.

Table S3. Synthetic DNA used to generate fragments with mutation.

Table S4. Primers used for PCR amplification of fragments cloned into pL66.